nature communications

Article

https://doi.org/10.1038/s41467-025-64888-9

Click-linking: a cell-compatible protein crosslinking method based on click chemistry

Received: 27 January 2025

Accepted: 30 September 2025

Published online: 06 November 2025

Check for updates

Bruno C. Amaral[1,3], Andrew R. M. Michael[1,3], Nicholas I. Brodie[1], D. Alex Crowder[1], Kristen H. Eiriksson[1] & David C. Schriemer[1,2]

Crosslinking mass spectrometry (XL-MS) has the potential to map the human interactome at high resolution and with high fidelity, replacing indirect, error-prone sampling methods such as affinity pulldown MS. However, the sampling depth of XL-MS remains stubbornly low. We present a crosslinking strategy that splits the crosslinking reaction into two sequential and orthogonal coupling events. The method involves pre-stabilizing the spatial proteome with a fixation protocol inspired by immunofluorescence imaging, followed by a stepwise process that begins with extensively labeling surface-accessible lysines in the cell with N-hydroxysuccinimide (NHS)-modified click reagents. We show that a subsequent copper-catalyzed azide-alkyne cycloaddition (CuAAC) reaction of the installed precursors generates crosslinks at levels approaching 30% of the total signal, as demonstrated by a subtractive approach. The method generates no detectable side reactions or obvious distortions of the spatial proteome. Protein-protein interactions (PPIs) are detected at levels approximately 20 times higher than a conventional DSS-based method, outperforming even enrichable crosslinkers.

Protein-protein interactions (PPIs) are a major organizational element in the cell. Mapping them as comprehensively as possible is necessary to understand the mechanisms behind every cellular process[1]. Mapping can be performed at different resolutions and scales. Structural techniques such as X-ray crystallography and cryoelectron microscopy provide the highest resolution and deliver the greatest mechanistic information about PPIs, but they have limited utility as a discovery tool and cannot be easily implemented at the cellular level. Techniques such as affinity pulldown mass spectrometry (AP-MS)[2] and Bio-ID proximity labeling[3] can be used for discovery, along with modern variants of yeast two-hybrid assays[4,5], but the structural resolution of these techniques is limited, and PPIs are only inferred from the resulting data. Most of these methods are labor-intensive when applied at the cellular scale, and they struggle to map and monitor dynamic interactions across time. We still need a robust technique that directly maps PPIs in cells, and one that is easy to use.

Crosslinking mass spectrometry (XL-MS) could be that superior method. It provides direct evidence of an interaction by defining a PPI based on a measured distance between two covalently bound proteins, through the insertion and detection of a bifunctional reagent of known length[6]. In situ crosslinking experiments have been moderately successful in PPI mapping[7,8]. PPIs have been detected that agree with existing interaction knowledgebases, and novel interactions are beginning to emerge, at least among proteins of higher abundance. Recent studies have even demonstrated that in situ crosslink measurements can support AI-driven structure modeling[9,10], raising the possibility of determining protein structures in the cell. Unfortunately, in situ applications of XL-MS do not deeply sample the interactome. Some success has been achieved, but these experiments are a significant undertaking in terms of time and cost, while still only producing modest numbers of PPIs[11–14]. The crosslinking step seems straightforward – simply bathing live cells with a solution of the

[1]Department of Biochemistry and Molecular Biology, University of Calgary, Calgary, AL, Canada. [2]Department of Chemistry, University of Calgary, Calgary, AL, Canada. [3]These authors contributed equally: Bruno C. Amaral, Andrew R. M. Michael. e-mail: dschriem@ucalgary.ca

crosslinking reagent – but the sample workup necessitates large amounts of lysate and elaborate detection methods. New approaches are needed.

There are at least two experimental issues to address. First, there is some uncertainty in the accuracy of PPIs identified via XL-MS, as kinetic trapping could generate non-native interactions. Second, the yields of crosslinking reactions are poor[15]. In a typical cell-based method, live cells are bathed with reagents and left to react for a long period of time (up to an hour), as a concession to the low membrane permeability of most reagents and the need to integrate reaction products to detectable levels. These conditions are not conducive to preserving cellular structures, nor to an error-free sampling of interactome dynamics. We recently showed that a pre-stabilized cell retains structure during subsequent crosslinking reactions, and reaction yields are improved at the same time[16]. This stabilization is achieved with high-concentration formaldehyde in a method inspired by standard immunofluorescence (IF) imaging. We simply replace the fluorescent stain post-fixation with MS-compatible crosslinkers. Prestabilization allows in situ XL-MS to inherit the same level of confidence in PPI detection as IF imaging. Any type of crosslinker can be introduced post-fixation, even membrane-impermeable ones. We call this method formaldehyde-enhanced in situ crosslinking MS (FIX-MS).

FIX-MS does improve performance, but crosslinking reaction yields are still not as high as they need to be. Yields hover around hundreds of PPIs even after extensive sample separation and enrichment, at least when beginning with low milligram amounts of protein[16]. Interactome coverage remains a small fraction of the estimated 650,000 pairwise protein interactions present in human cells[17]. We were interested to see if reaction yields could be improved and there are reasons to think that it is possible. Typical NHS-based amine-targeting reagents, by far the most common, can partially hydrolyze during the crosslinking reaction and block otherwise linkable lysines. These reagents may also interact with other biomolecules, and even self-compete[18]. Thus, monolinks are the dominant product[15]. This problem occurs because crosslinking methods use one molecule with two identical reaction groups, in a concerted reaction.

Uncoupling the stabilization of the cell from the insertion of crosslinks provides an opportunity to reinvent in situ crosslinking. We propose to separate crosslinking into two orthogonal reactions (Fig. 1A). For example, a first coupling event could support the labeling of surface-accessible lysines, followed by a washing step to remove the remaining reactants and at least some reaction byproducts (*i.e.*, hydrolyzed reagents). Initiation of the second coupling, which creates the crosslink, could then occur in an environment where insertion yields can be measured and controlled, and any competition is only between inter- and intra-protein linkage events. Here, we investigate this concept using click chemistry as the second reaction and test its merits. We demonstrate that this click-linking approach is compatible with the FIX-MS protocol and highlight the potential of the method for deep PPI sampling.

Results and Discussion

Deconstructing the crosslinking reaction

Separating crosslinking into two sequential reactions first requires the selection of orthogonal coupling chemistry (Fig. 1B). We chose N-hydroxysuccinimide (NHS) esters for the first step, to selectively bioconjugate free amines in lysines and protein N-termini. Retaining a high degree of selectivity on the primary coupling will facilitate the detection of any cross-links that we create, as database searches can be targeted to a reduced set of residues. While other chemistries are certainly possible (e.g., coupling to carboxylic acids), NHS esters are very reactive, and a wide range of coupled, secondary reactive groups are readily available. We selected reagents that enable copper(I) catalyzed azide-alkyne cycloaddition (CuAAC) reactions[19]. This click reaction generates 1,2,3-triazoles that are stable in solution and during MS analysis. The reaction is highly selective, and its precursors are chemically compatible with NHS esters. The two precursors, when clicked, would form a reagent with a total spacer length of approximately 18 Å, only slightly longer than most conventional crosslinkers.

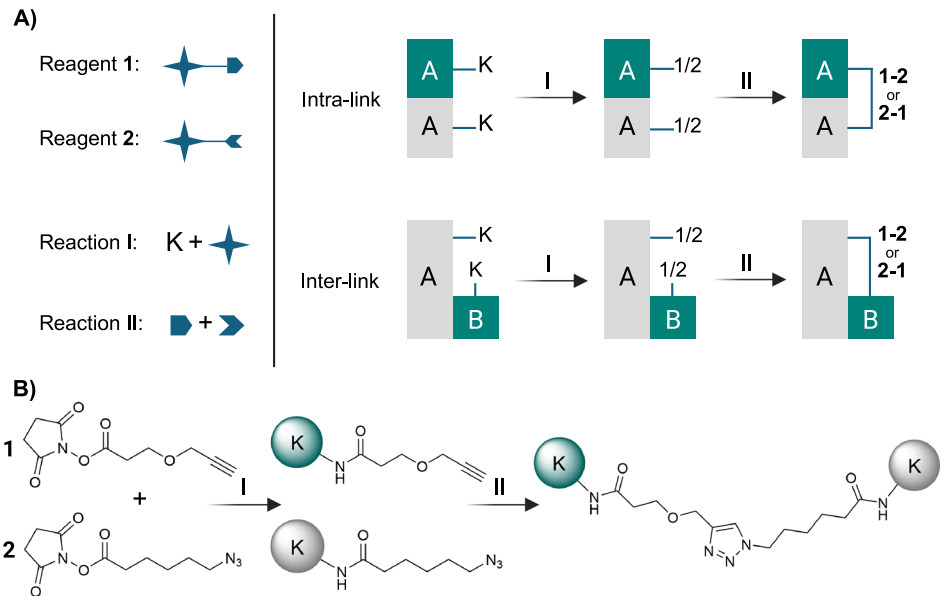

Fig. 1 | Deconstructing the crosslinking reaction. A Conceptual approach to deconstructing protein crosslinking into two orthogonal reactions. To illustrate, the first reaction can target amines, where both reagents **1** and **2** compete for available lysines. When admixed in a 1:1 molar ratio and applied to a stabilized cell, the reagents can label all accessible lysines with controllable yields. Each amine will possess a 1:1 ratio of the products of **1** and **2**. In the two examples provided, an intralink or an interlink will form after initiation of the orthogonal reaction, to a maximum of 50% of the bioconjugation yield (assuming linkage to only one proximal amine is possible). Asymmetry in the second reaction would lead to two reaction products (same mass, different orientation). **B** Click-linking reaction scheme used in this work. 2,5-dioxopyrrolidin−1-yl 3-(prop-2-ynyloxy)propanoate (**1**) and (2,5-dioxopyrrolidin−1-yl) 6-azidohexanoate (**2**) contain NHS esters for a standard lysine bioconjugation (reaction I). Reaction II is based upon copper-catalyzed azide-alkyne cycloaddition (CuAAC), using Cu(I) and BTTES.

https://doi.org/10.1038/s41467-025-64888-9

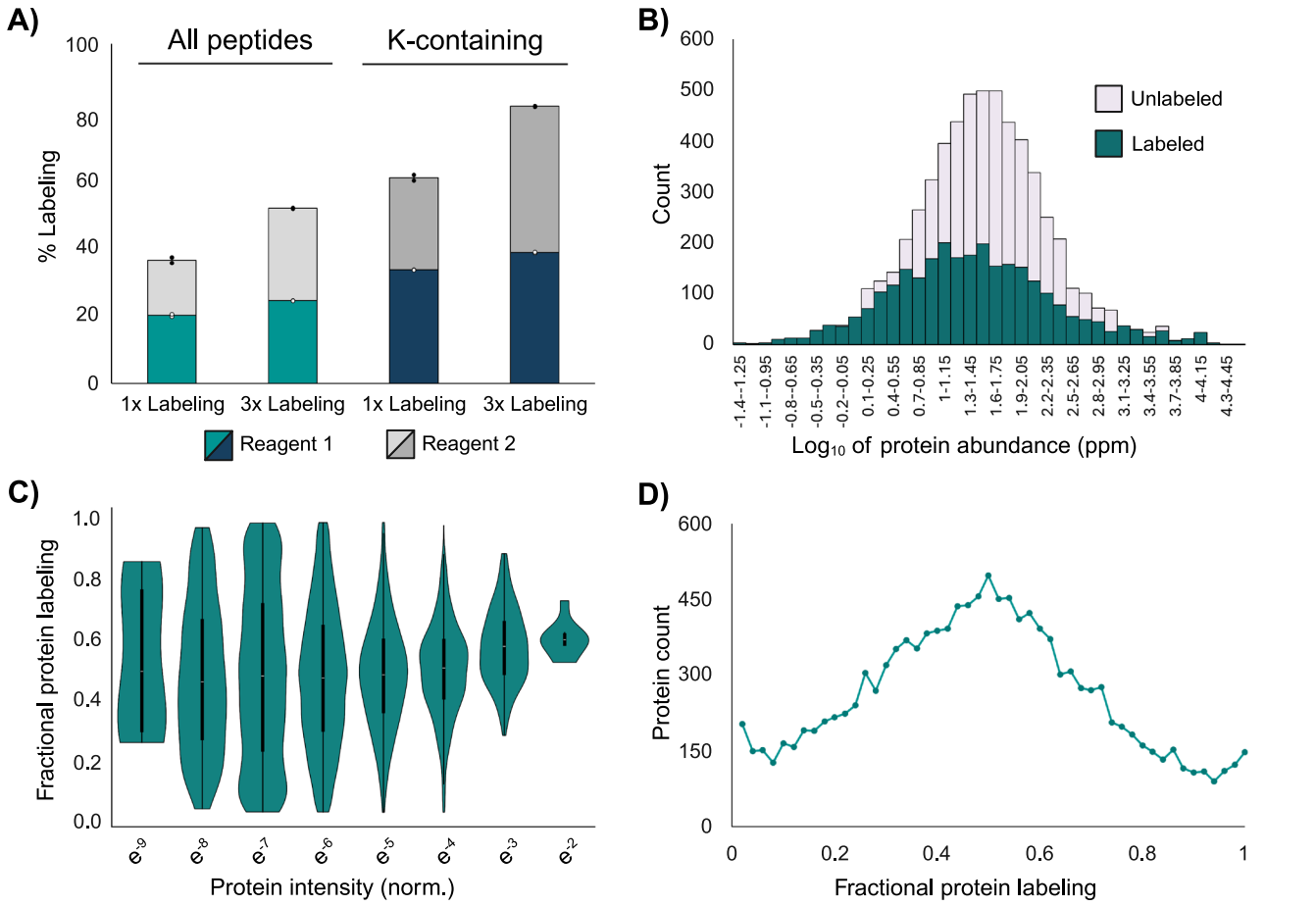

Fig. 2 | Properties of the initial NHS-based bioconjugation reaction. A Labeling levels achieved in a single application of a 1:1 molar ratio of reagents **1** and **2**, calculated by using all detected peptides as well as only the lysine-containing peptides. Labeling is expressed as fraction of total labeled peptide intensities over all peptide intensities for a given peptide class. Data showing a single application of reagent mix (1x) and three sequential applications of the reagent mix (3x). **B** Proteome-level distribution of labeling for the 1x application, relative to an unlabeled proteome analyzed in the same manner. A protein was counted as labeled if one or more labeled lysine-containing peptides was detected. Protein abundance estimates from PaxDB[45]. **C** Data as in B, with violin plots showing the distribution of fractional protein labeling (total labeled lysine-containing peptide intensity over total peptide intensity for given protein) as a function of protein abundance (estimated from peptide intensities normalized to total ion intensity). **D** Data as in (**B**), showing a distribution of per-protein fractional labeling levels. For all panels, $n = 2$ biological replicates. Source data are provided as a Source Data file.

A catalyzed reaction is essential. The precursors must remain inert during bioconjugation in the absence of the catalysts, and only be active in the subsequent step when the catalysts are added. Cu(I), together with activating ligands, increases the reaction rate by approximately 7 orders of magnitude[19,20]. Cu(I) is cytotoxic to live cells, but this is a non-issue, as cells are fixed with formaldehyde at the start of the procedure.

The two precursors can be installed simultaneously in a 1:1 molar ratio. Barring any insertion bias, every free amine would possess an equimolar amount of each click precursor, and the crosslinking yield would be no worse than 50% of the combined insertion levels. For a single crosslinkable pair of lysines, azide would not couple to azide, nor alkyne to alkyne, but if the number of nearby linkable lysines increases, the crosslinking yield can approach 100%. For example, six linkable lysines proximal to a labeled lysine site would generate a 98.4% maximal crosslinking yield at the site.

The reaction – step one

We fixed and permeabilized human A549 cells using the conventional FIX-MS approach, and then added 2,5-dioxopyrrolidin-1-yl 3-(prop-2-ynyloxy)propanoate (**1**) and (2,5-dioxopyrrolidin-1-yl) 6-azidohexanoate (**2**) in equimolar amounts. A combined concentration of 2 mM and a 60 min reaction time generated a high level of labeling. Using peptide intensity as a measure, 36% of the total signal arises from labeled peptides, or 61% when counting only lysine-containing peptides. This level can be boosted with repeat applications of the reagents to improve depth of labeling (Fig. 2A). We used the "1x" application of reagents for the rest of the reaction assessment.

Approximately 90% of the labels that we install are on surface-exposed lysines, estimated by probing the reagent-accessible surface area (RASA) of several thousand AlphaFold protein models, although we note that the two reagents do not perfectly overlap in the lysines that they label (Supplementary Fig. 1). Nevertheless, the bioconjugation yields for the two reagents are nearly equal. Minor deviations likely reflect dispensing errors, the insertion bias, and/or unequal identification probabilities for peptides that contain different modifications. The labeling depth is broadly reflective of the composition of the proteome. We appear to sample across the full range of protein expression (Fig. 2B). The modified peptides are shifted towards the lower abundance elements of the proteome, but the shift is modest and likely arises due to altered digestion patterns. Labeled peptides render lysines resistant to trypsin and could shift the detection properties of the proteome. The labeling yields for individual proteins are variable, but the average labeling per protein is generally independent of protein abundance (Fig. 2C, D).

https://doi.org/10.1038/s41467-025-64888-9

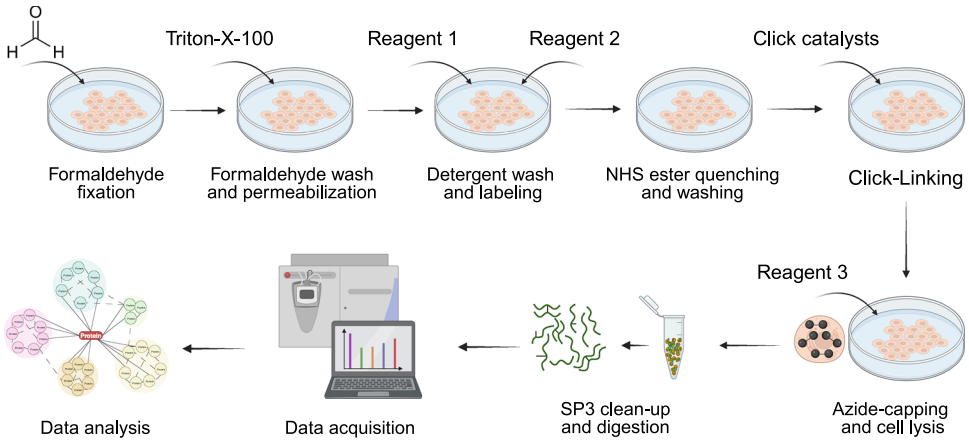

Fig. 3 | Schematic of the multistep click-linking workflow. Cells are first stabilized with high-concentration formaldehyde and then permeabilized to allow for the simultaneous introduction of two reactive click precursors. After bioconjugation and washing, CuAAC catalysts are added to complete the crosslink. After capping any remaining free azides, cells are harvested for sample workup. Reagent 1: 2,5-dioxopyrrolidin-1-yl 3-(prop-2-ynyloxy)propanoate. Reagent 2: and (2,5-dioxopyrrolidin-1-yl) 6-azidohexanoate. Reagent 3: 11,12-didehydro-γ-oxodibenz[b,f]azocine-5(6H)-butanoic acid. Created in BioRender. Schriemer, D. (2025) https://BioRender.com/p82h674.

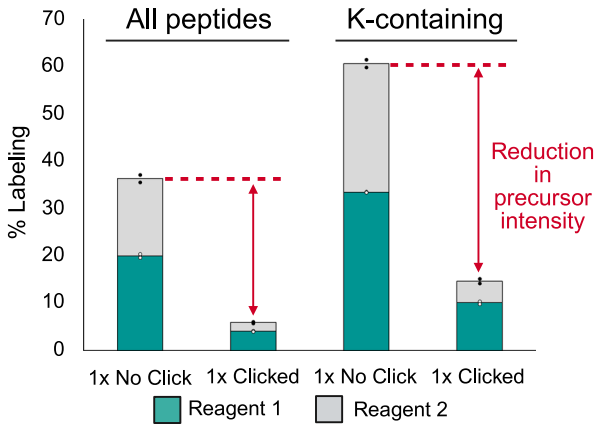

Fig. 4 | Effect of the click reaction on the abundance of detectable click precursor peptides. The reduction in detectable labeled peptides is expressed as a fraction of the total detectable signal and stated for all peptides and those only containing lysines ($n = 2$ biological replicates). Source data are provided as a Source Data file.

We noted a strong bias against azide-modified peptides initially, but we speculated that these peptides experienced a greater level of loss during sample workup. Thus, we capped the bioconjugated azides before sample workup, using 11,12-didehydro-γ-oxodibenz[b,f]azocine-5(6H)-butanoic acid (DBCO-acid). DBCO-acid is a very reactive strained alkyne that reacts with azides in a spontaneous strain-promoted alkyne-azide cycloaddition (SPAAC) reaction[21]. This capping returned detectability to the azides. No additional products of the bioconjugation reactions were found in an open-modification search, confirming the high selectivity of the reaction.

The reaction – step two

We then explored the effect of catalyst composition and reaction time on the ability to achieve an efficient click reaction, initially using cell lysates and a "half reaction". That is, we installed **1** alone into either *E. coli* or A549 cell lysates, and then added 2-[2-(2-azidoethoxy)ethoxy]-ethanol as a capping reagent. These monovalent modifications are much easier to detect with current proteomics methods than cross-links. Classical CuAAC ligands such as THPTA, while effective, are strongly hydrophobic and interfere with LC-MS analysis. Additionally, they require high concentrations of organic solvent in the reaction and could possibly induce cellular distortion, even after fixation. Thus, we used a newer generation ligand, 3-(4-((bis((1-(*tert*-butyl)-1*H*-1,2,3-triazol-4-yl)methyl)amino)methyl)-1*H*-1,2,3-triazol-1-yl)propane-1-sulfonic acid (BTTES), which is water soluble[22]. Aside from this one change, standard CuAAC reaction conditions proved highly effective, leading to a near-quantitative conversion of the propargyl group to the triazole in 15 min using a 2:1 ratio of ligand to Cu(I) (Supplementary Fig. 2). The reaction time can be even shorter, but we elected to use 15 min as a default for all subsequent experiments. Based on an open modification search (Supplementary Data 1), we did not observe any side products in the proteome, consistent with the bioinert nature of the CuAAC reaction. We note that a very minor thiotriazole product could form with proximal cysteines, but it would be difficult to detect[23]. We next tested this click-linking reaction on bovine serum albumin (BSA) and detected 582 crosslinks (519 intralinks and 63 loop links), which compare favorably to a standard DSS crosslinking reaction of BSA that, in our hands, returns 362 crosslinks (302 intralinks and 60 loop links) (Supplementary Fig. 3).

Click-linking – in situ click reaction of installed precursors

Using the reaction as described above, we then explored the effectiveness of the entire click-linking process, from fixation to installation of the click precursors, and then to the final cycloaddition reaction to create the crosslinks (Fig. 3). We chose a subtractive approach to evaluate performance. That is, we monitored the drop in the level of detectable click precursors because, as noted above, monovalent modifications are much easier to enumerate than crosslinked peptides. We reasoned that quantifying the drop in monovalent modifications would support a more accurate first estimate of crosslink success. The drop was substantial and reproducible (Fig. 4). In the 1x labeling experiment, the alkyne-modified peptides dropped by 80% and the azide-modified peptides by 89%.

We then considered what other biomolecules might possibly compete with the formation of protein crosslinks. We do not expect DNA or RNA to contribute crosslinkable sites, as they are not reactive to NHS esters. While it is possible that amine-containing metabolites could compete with proteins, the cross-linking process should deplete the cell of metabolites, as multiple washing steps are incorporated post-fixation. To test this, we extracted the metabolome from fixed

https://doi.org/10.1038/s41467-025-64888-9

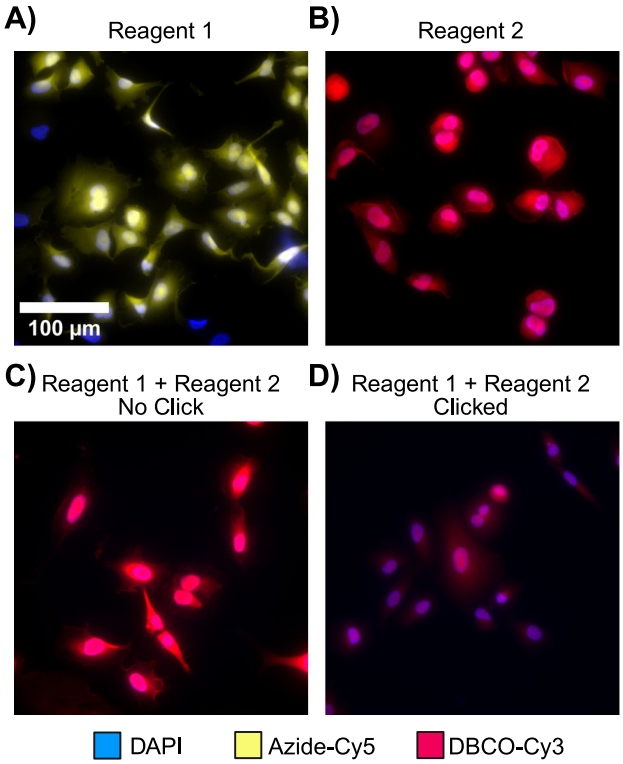

Fig. 5 | Distribution of installed precursors and effect of the click reaction on the abundance of fluorescence signal. A549 cell cultures were treated individually with **A** the alkyne reagent **1** and then clicked to Azide-Cy5 (**B**) the azide reagent **2** and then clicked to DBCO-Cy3. For quantitating crosslinking, A549 cell cultures were treated with both precursors, then coupled with DBCO-Cy3 either **C** before or **D** after precursors were clicked together through click-linking. Fluorescence signal is reduced after clicking and is correlated to lower azide availability due to crosslink formation (see methods). Source data are provided as a Source Data file. Representative images from five fields of view (n = 1 biological replicate).

and permeabilized cells and performed a quantitative metabolomics analysis of amine-reactive metabolites. We used live cells as a control, to represent the conventional in situ crosslinking reaction. The metabolite levels are very high in the control, but the click-linking workflow reduces the amine-reactive pool of metabolites to nearly undetectable levels (Supplementary Fig. 4). Interestingly, side reactions with metabolites are not seen in the conventional method. There are hundreds to thousands of amine-containing metabolites in a cell, thus signal splitting would likely render them undetectable in typical experiments. Taken together, the reduction in click-link precursors that we observe in Fig. 4 appears solely due to the production of intraprotein and interprotein crosslinks, suggesting a very high-yielding reaction of approximately 30% for the 1x reaction, considerably higher than the 0.1% estimate from previous studies of conventional crosslinking methods[15]. We tested this estimate using a fluorescence imaging strategy (Fig. 5). First, we treated A549 cell cultures separately with reagents **1** and **2**. We then clicked these with Azide-Cy5 and DBCO-Cy3, respectively. The resulting labeling confirms that the reagents are widely distributed throughout the cells. Second, click-link precursors were installed together in two matched cultures of A549 cells, and to one culture we added Cy3-labeled DBCO. This reagent spontaneously reacts with azides, as noted earlier. To the other culture, we completed the click-linking procedure and then probed for residual azide with Cy3-DBCO. We also observed strong pan-cellular labeling in the pre-clicked sample, confirming that the precursors are well distributed throughout the proteome. Fluorescence intensity dropped to 30.4% of the initial after the click reaction, which is generally consistent with the MS-based quantitation of crosslink yield (Fig. 4).

Click-linking does not distort cellular ultrastructure

We previously showed that the spatial proteome remained stable over multiple successive applications of crosslinker during FIX-MS[16]. However, the process of click-linking is slightly different than FIX-MS. If reversible formaldehyde crosslinks between amines form the basis for proteome stabilization[24], then it is possible that an extended treatment with the NHS-based click precursors could outcompete the formaldehyde crosslinks and destabilize the cell. To evaluate this, we fixed and permeabilized A549 cells as usual, and then treated them with the 1:1 molar ratio of reagents **1** and **2** (total concentration of 2 mM) for a total of 60 min. We then imaged the cells using CF647-phalloidin staining to observe the effect on the actin cytoskeleton, a structurally sensitive state that is coupled with many cellular processes[25]. The cells remained fixed and stable relative to an unlabeled control (Fig. 6A). Interestingly, this experiment indicates that reversible lysine-formaldehyde crosslinks do not appear to significantly contribute to the fixation process used in click-linking.

We then explored the effect of the click reaction. However, we were not able to sensitively image the actin cytoskeleton after introducing the click catalysts, as Cu(I) appears to interfere with phalloidin staining[26,27]. We treated the cells with EDTA to chelate and wash away soluble copper after click-linking. This process restored some of the signal, sufficient to indicate that the ultrastructure is preserved, but it was difficult to accurately quantify cell distortion (Fig. 6A). To confirm stability we stained for microtubules, another dynamic element of the cytoskeleton, after confirming that staining levels are unaffected by the reagents used in the click-linking process. There is no obvious change in microtubule structure upon click-linking. Even the fragile machinery of the mitotic spindle in metaphase is preserved (Fig. 6B), supporting our observation that the spatial proteome remains stabilized during click-linking.

Click-linking outperforms standard crosslinking and FIX-MS

We then processed the 1x click-linked A549 cells for XL-MS experiments, to compare crosslinking performance with two other well-known NHS-based crosslinking reagents, DSS and PhoX. We chose non-cleavable reagents so that the database search routines and parameters would be comparable. DSS is a conventional non-enrichable reagent while PhoX is a highly-enrichable reagent[28]. Both were implemented using the FIX-MS process to increase insertion yields, and we also included a conventional live-cell treatment with DSS for comparison (data retrieved from an earlier study[16]). Click-linking generates CSMs and unique crosslinks that are slightly higher in number than DSS installed by FIX-MS, but the distribution of reaction products is quite different (Fig. 7A,B). Click-linking generates a much larger ratio of structurally informative crosslinks. Fully 60% of the crosslinks are useful distance measurements (inter and intraprotein crosslinks), compared to 20% for DSS and 31% for PhoX. Indeed, while click-linking generates 60% less crosslinks than PhoX, the number of PPIs is greater (Fig. 7C). This is a remarkable result given that click-linking does not incorporate a strong enrichment mechanism like PhoX.

There are at least two reasons for an improvement in PPI sampling relative to looplinks. First, the click-linked product is longer than DSS (11.4 Å) and PhoX (5 Å), which may generate more intra- and inter-protein crosslink reactions. Second, the regioselective click reaction involves transition states that may be sterically unfavored when two click-linking precursors are installed very close to each other on the same protein[29]. Additional reagent synthesis will help uncover if this observation is unique to click-linking. As the complexity of the reaction products is very high in XL-MS (and these products all compete for finite MS detection time) any tilt towards a higher percentage of interprotein crosslinks should improve PPI detection.

https://doi.org/10.1038/s41467-025-64888-9

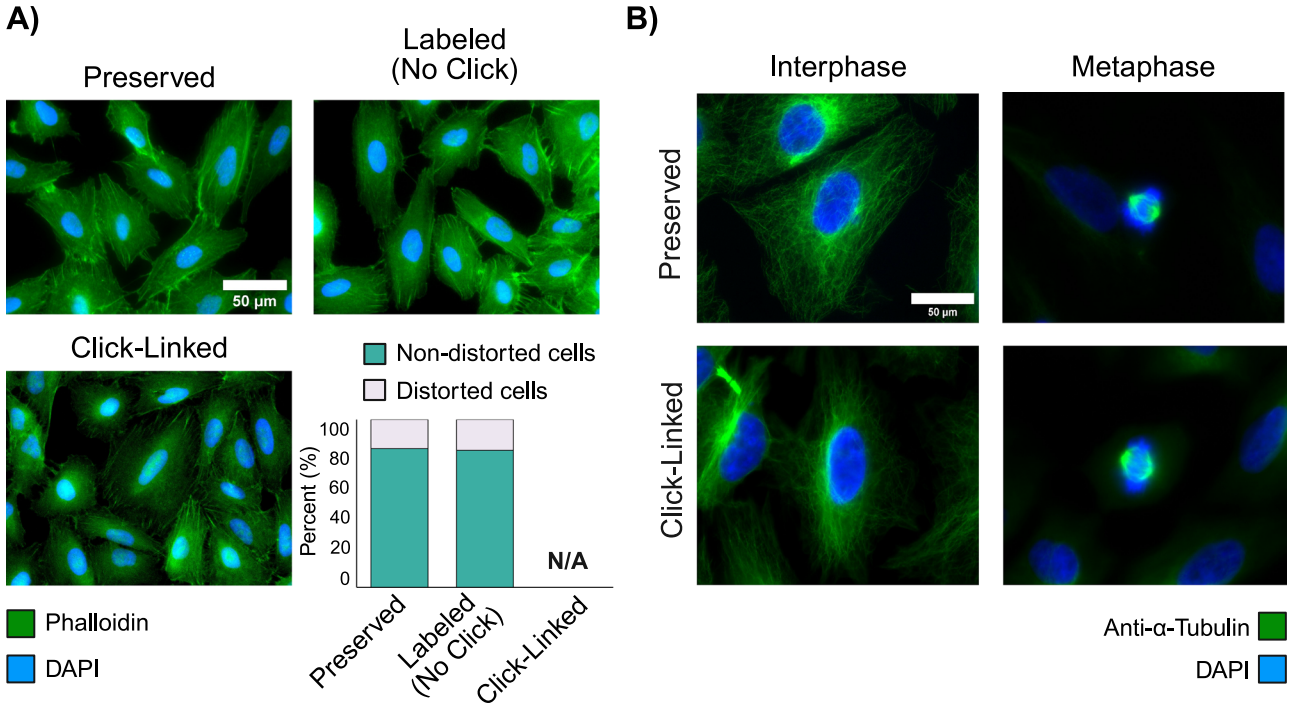

Fig. 6 | Click-linking does not negatively affect the ultrastructure of the cell. **A** A549 cells imaged using CF647-phalloidin staining (filamentous actin, pseudo-colored green) and DAPI (nucleus, blue), after a standard cellular fixation protocol (top left), insertion of click precursors **1** and **2** to a 50% labeling level (top right), and after clicking and an EDTA wash (bottom left). Enumeration of cellular integrity in bottom right, based on defined metrics for integrity (see methods). **B** A549 cells imaged using an FTIC-anti-α-tubulin antibody (green) and DAPI, after a standard cellular fixation protocol showing both a cell in interphase (top left) and mitotic cell in metaphase (top right). Cells imaged after the full click-linking protocol, also showing a cell interphase (bottom left) and a mitotic cell in metaphase (bottom right). Source data are provided as a Source Data file. Experiments performed in duplicate, >100 cells used for distortion evaluation.

In-depth analysis of the in situ click-linking reaction

These click-link precursors are not yet enrichable, thus linear free peptides still comprise the largest fraction of identifications from a typical experiment, even for click-linking (86%, Supplementary Data 2). We added an additional fractionation step to the workflow as partial enrichment (although this extra dimension is not as effective as the IMAC enrichment used for PhoX) and then measured the number of PPIs with an equally modest sample input (~10 mg of protein as starting material). Specifically, we used size-exclusion chromatography (SEC) to fractionate the protein extract from a typical click-linking experiment. We generated five SEC fractions and then separated each fraction into additional fractions using high-pH reversed-phase chromatography, prior to LC-MS/MS (see methods). This effort identified 1700 PPIs, five times greater than PhoX, and the advantageous distribution of reaction products was preserved (Fig. 7A–C).

We evaluated these 1700 PPIs against the STRING database and noted that, while a large fraction was corroborated with high STRING scores, an even larger fraction was not found in the database. This ratio is reproducible and generally independent of how the datasets were collected (Fig. 7D). However, the fraction of PPIs not found in STRING is higher for click-linking than for PhoX. There could be several reasons for this higher ratio. Click-linking might generate a higher error rate using our chosen database search tool (pLink2). Additionally, if protein movement is not fully restricted during fixation, indirect interactors could be linked. However, local diffusion should also negatively affect the PhoX-based method, but it does not appear to do so, as the ratio for PhoX is lower. We note that DSS crosslinking generates a "not found" fraction of PPIs similar to click-linking, thus it is possible that the large number of linear peptides in these experiments confound the search algorithms, which PhoX suffers to a lesser extent because it is enriched.

But it is also possible that we are sampling a number of undescribed PPIs, as the STRING database is not comprehensive. It is impractical to validate all 990 entries in this class, thus we sought to globally estimate boundaries on the error rate. We analyzed the gene ontology (GO) for the proteins comprising each PPI, reasoning that crosslinked proteins would derive from a common cellular compartment. Localized diffusion (if it occurs) should not scramble this basic GO term. An analysis of all hits with a STRING score greater than zero showed that 667/710 (94%) of the PPIs were comprised of proteins drawn from the same cellular compartment, suggesting its utility as a filter. A random sampling of proteins in the proteome returns a 21% likelihood that PPIs will have components with a shared cellular compartment purely by chance. We find that 482/990 (49%) of the PPIs in the not found category have proteins in a shared compartment. This analysis suggests that 28% of the PPIs in the not found category could be correct. Therefore, in the aggregate, together with a 5% FDR estimate established at the search level, we can estimate that 58-95% of the PPIs we detect in this set are true positives. The DSS-based crosslinking methods generate a similar range (Supplementary Data 3). We then investigated the global spectral quality of crosslinks supporting the entries in the not found category and observed that 47-58% of the CSM scores were better than 0.5 (moderate to high quality, Supplementary Fig. 5). Interestingly, click-linking CSMs scores are superior to PhoX, although PhoX generates hits in the 76-95% range based on shared compartments.

Finally, we performed a search of all the crosslinking data using CRIMP 2.0 and MS Annika 3.0, two conservative tools for PPI detection[30,31], and we repeated the analysis with pLink 3.0.17 (which has improved error control over version 2 and was released during revisions to the manuscript). Fewer PPIs were detected, but all tools generated the same trend: click-linking outperformed all other crosslinking strategies, and a sizable fraction of PPIs were in the not found category (Supplementary Fig. 6). Interestingly, although these software tools have improved error control, the PPI overlap between

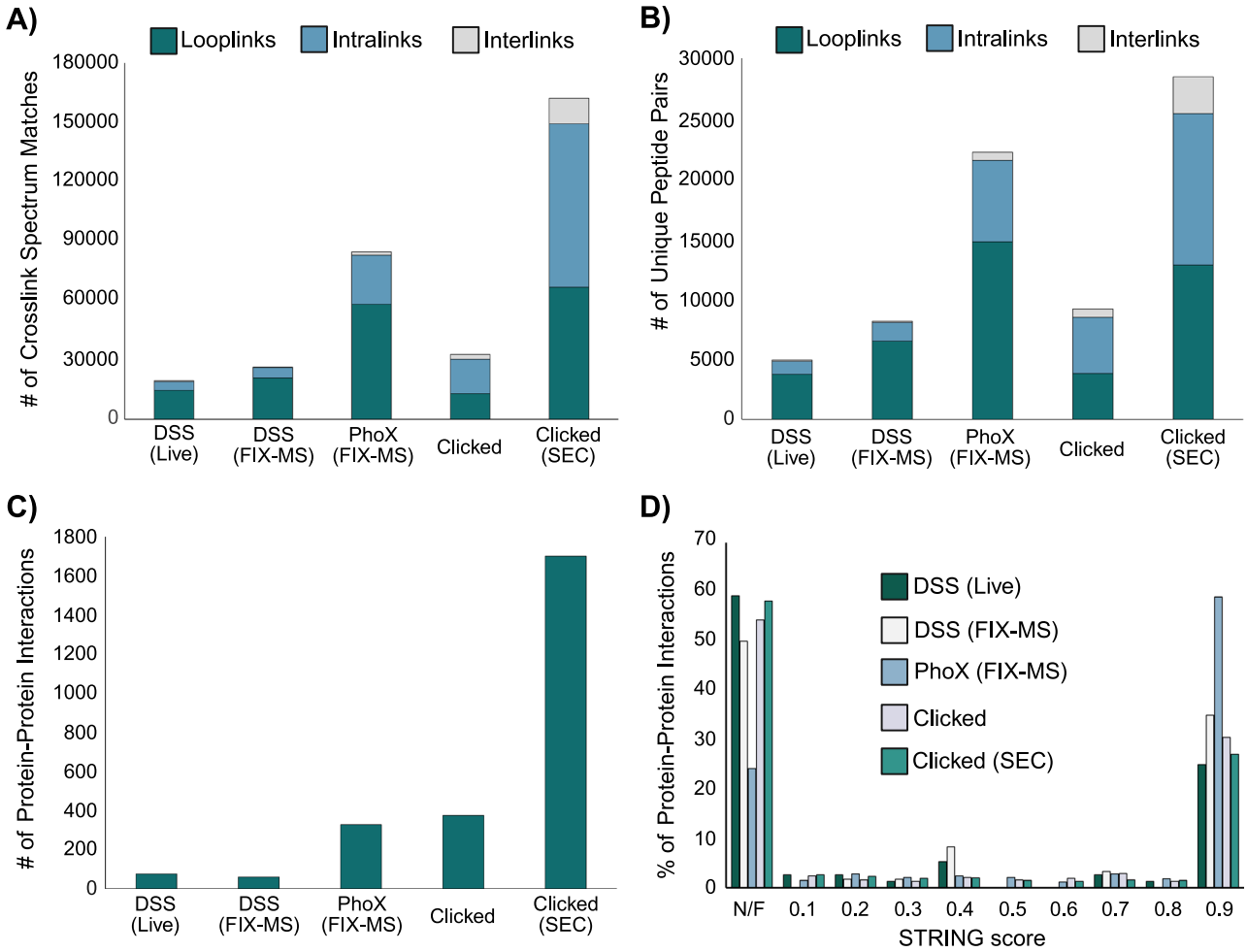

Fig. 7 | Comparing click-linking to alternative in situ XL protocols. A Number of crosslinked spectrum matches (CSMs) for a range of methods: live cells crosslinked in the conventional fashion with DSS, DSS and PhoX applied in a FIX-MS protocol, and the click-linking protocol. Click-linking results are also shown with an extra dimension of separation applied (size exclusion chromatography, SEC). **B** as in A, bur for unique crosslinked peptides. **C** As in A but displaying the number of unique PPIs detected. **D** Cross-referencing the PPIs detected by all methods against the STRING database. N/F means "not found". Source data are provided as a Source Data file.

tools was not high even in the high-scoring STRING subset, suggesting that scoring algorithms are differentially sensitive. Taken together, the click-linking protocol likely identifies hundreds of unmapped PPIs, generating data that are superior in quality and quantity to PhoX data, even though affinity enrichment was not used.

Finally, we illustrate that click-linking does faithfully sample protein structure and capture interactors that reflect biological function. We tested the integrity of sampling by mapping the crosslinks to available protein structures using CLAUDIO[32]. Of the 14,527 crosslinked peptide pairs identified, CLAUDIO was able to map 7805 across 1482 protein structures (the vast majority involving monomeric proteins), reflecting good structural sampling. Over 87% of these measured crosslinks mapped to within 35 Å (Supplementary Fig. 7). As an example of a functional complex, we identified ACIN1, a nuclear protein that is crosslinked to SAP18 (a histone deacetylase complex subunit) and RNPS1 (RNA-binding protein with serine-rich domain 1) that together form the apoptosis and splicing-associated protein (ASAP) complex[33,34]. This sub-structure is part of a larger exon-junction complex (EJC) that regulates gene expression after transcription. Evidence for this is found in cross-links between SAP18 and the Pinin splicing factor[35,36]. An AlphaFold Multimer model of the ternary complex supports the measured interprotein crosslinks, except for those situated in the highly disordered regions (Supplementary Fig. 8).

In summary, click-linking is a very effective protocol for increasing the yield of protein crosslinks, and one that avoids the weaknesses of the traditional method. There are many reasons for the improved yield. In the first place, the method promotes greater control over the chemical reaction itself. Pre-stabilizing the proteome allows us to wash away partially hydrolyzed click precursors as well as labeled metabolites, both major classes of competing reaction products. Additionally, self-competition is avoided[18]. That is, if two linkable residues are each labeled with a conventional homobifunctional crosslinker, they cannot crosslink. In click-linking, competition can only occur in the second reaction, but this will always generate a protein crosslink.

While the yields are clearly superior to other methods, it is somewhat surprising that PPI detection is not higher than the numbers we presented, given that our yields are significantly increased. The reasons for this are complex and the subject of a separate investigation, but we note here that search engines are not yet well optimized for searches of this scale. Nevertheless, combining cellular fixation with multistep reactions provides clear benefits over the classical crosslinking method, and illustrates a generic strategy that can be extended to many other reagent combinations in the pursuit of deep interactome sampling.

Methods

Cell culture

E. coli (DH5α) cells were seeded into 50 mL of 2YT + Amp100 (Fisher Scientific) medium and grown overnight at 37 °C, extensively washed with 1X PBS and lysed for the click optimization experiments. A549

cells (American Type Culture Collection (ATCC), catalogue No. CCL-185) were cultured in Ham's F-12K medium (Gibco) supplemented with 10% fetal bovine serum (FBS, Gibco) and 1% penicillin-streptomycin (Gibco) at 37 °C in a humidified atmosphere with 5% CO_2. For imaging experiments, cells were seeded in a 1 cm microscope coverslip and grown to 80% confluency. For labeling and crosslinking experiments, they were seeded in 10 cm Petri dishes and grown to the same confluency.

Cell fixation and permeabilization

Cells had growth medium removed and were washed with 1X PBS buffer at pH 7.4. A 4% (v/v) formaldehyde solution in 1X PBS was freshly prepared and added to the cells for fixation. The incubation was held at 25 °C for 10 min and excess formaldehyde solution was washed away with 1X PBS. Cells were then treated with a solution of 0.1% (v/v) Triton-X-100 in 1X PBS for 10 min at 25 °C. The surfactant was then washed out prior to labeling experiments.

In situ monovalent labeling reactions

Fixed and permeabilized cells were washed three times with 1X PBS, then treated with both monovalent reagents simultaneously, at a final 1 mM concentration for each. Stock solutions of both (2,5-dioxopyrrolidin-1-yl 3-(prop-2-ynyloxy)propanoate, Reagent **1**, Sigma Aldrich #764221) and (2,5-dioxopyrrolidin-1-yl) 6-azidohexanoate, Reagent **2**, Vector Laboratories #CCT-1402) were prepared to 100 mM in anhydrous DMSO, then pre-mixed before adding to the plates. Reactions were carried out for 60 min at 25 °C under gentle mixing, before quenching with 20 mM ammonium bicarbonate. Excess reagents were washed out with 1X PBS, and free azido groups were capped with 1 mM (11,12-didehydro-γ-oxodibenz[b,f]azocine-5(6H)-butanoic acid, DBCO-Acid, BroadPharm #CCT-1117). Cells were harvested from the plates in a lysis buffer composed of 100 mM Tris(Hydroxymethyl)aminomethane, 150 mM sodium chloride, 1% (v/v) Triton-X-100, and 2% (v/v) sodium dodecyl sulfate, at pH 7.8.

Click optimizations

For the click optimization conditions, either *E. coli* or A549 cells were cultured as described above, and the lysate was taken for labeling. 100 μg of pre-reduced and alkylated lysate (see Sample work-up below) were bound to and cleaned up following the standard SP3-protein protocol. Instead of proceeding to the digestion step, the bead slurry was resuspended in 500 μL of 1X PBS, and proteins were treated with 1 mM Reagent 1. Labeling reaction was carried out for 60 min at 25 °C under strong mixing to keep the beads in suspension, followed by quenching with 20 mM ammonium bicarbonate, mixing for another 10 min at 25 °C. Excess reagents were washed out from beads, which were resuspended again in 500 μL of 1X PBS. Labeled proteins were then treated with 1 mM 2-[2-(2-azidoethoxy)ethoxy]-ethanol (ConjuProbe, #CP-1218) with no click-catalysts present. For the time-course, copper sulfate, 3-(4-((Bis((1-(tert-butyl)-1H-1,2,3-triazol-4-yl)methyl) amino)methyl)-1H-1,2,3-triazol-1-yl)propane-1-sulfonic acid (BTTES, Vector Laboratories, #CCT-1237) and sodium ascorbate were premixed and introduced together to the solution at 5, 10, and 50 mM, respectively. Reactions were quenched at the specific time points with 10 mM DBCO-Acid. For the reagent ratio optimization, copper sulfate and sodium ascorbate were maintained at 5 and 50 mM, respectively, while BTTES was tested in different concentrations. The click-chemistry reaction was conducted for 15 min at 25 °C under strong mixing, before being quenched with 2 mM DBCO-Acid. Excess reagents were washed out from beads and proteins were digested with trypsin as described below.

In situ Click-Linking reactions

Cells were fixed, permeabilized and labeled with both reagents using the same conditions as above. After quenching the excess NHS esters and washes to remove excess reagent, the click-chemistry catalysts were added. Copper sulfate, BTTES and sodium ascorbate were premixed and added together to the cells for final concentrations of 5, 10 and 50 mM, respectively. The clicking reaction was carried for 15 min at 25 °C under gentle mixing. Excess reagents and click-catalysts were washed away with 1X PBS, and 1 mM DBCO-Acid was added to cap any remaining free azido groups and prevent any downstream unwanted click reactions. Cells were then collected and lysed as described above.

Fluorescence imaging of labeled cells

A549 cells grown on glass coverslips were washed with 1X PBS, then fixed and permeabilized as described above. Cells were treated with 1 mM reagent **1** and/or 1 mM reagent **2**, depending on the experiment. For samples labeled solely with reagent **1**, cells were treated with a mixture of 1:99 Cy5-azide (Sigma Aldrich, #777323): 2-[2-(2-azidoethoxy)ethoxy]-ethanol and the click catalysts at the same ratios as above. For samples labeled solely with reagent **2**, cells were treated with a mixture of 1:99 DBCO-Cy3 (Sigma Aldrich, #777366): DBCO-Acid. For samples labeled with both reagents, cells were treated with a mixture of 1:99 DBCO-Cy3:DBCO-Acid either before (No Click) or after (Clicked) the crosslink formation with the click-catalysts to monitor a drop in fluorescence signal by reduction of available free precursors. Cells were mounted with EverBrite + DAPI mounting medium (Biotium) for easy localization and DAPI signal normalization under the microscope. Fluorescence images were acquired on a LMD7 Laser Microdissection Microscope (Leica Microsystems) using a 40X objective and standard filter sets for DAPI (390/435 nm), Cy3 (554/594 nm), and Cy5 (636/695 nm). Image processing and fluorescence quantification were performed in Fiji (ImageJ), with signal intensity measured as mean gray values.

Sample work-up

All cell lysates were submitted to reduction of cysteines by incubation with 10 mM DTT at 52 °C for 30 min, followed by alkylation with 40 mM CAA at 25 °C for another 30 min in the dark. Reduced and alkylated lysate was bound to and cleaned up using the SP3-protein protocol. On-bead labeling experiments were performed at this point as described above, while samples where labeling and crosslinking occurred in situ proceeded directly to digestion. Digestion with trypsin in 50 mM ammonium bicarbonate, pH 7.8, at a 1:50 (w/w) trypsin-to-protein ratio was carried at 37 °C for 16 h. A small aliquot of each sample was collected and desalted with C_{18} ZipTips (Millipore Sigma) and submitted to LC-MS/MS for the analysis of percent labeling and general quality control. The remaining samples were desalted using Pierce Peptide Desalting Columns (ThermoFisher Scientific) and submitted to fractionation.

Fractionation

Samples were fractionated using a Vanquish Online 2D-LC system (ThermoFisher Scientific). For High-pH reverse phase fractionation, desalted peptide samples were resuspended in high-pH Mobile Phase A (20 mM ammonium formate, pH 10) and loaded onto a ZORBAX RRHD Extended-C_{18} column (80 Å pore size, 2.1 × 150 mm, 1.8 μm particles, Agilent). Separation was performed in a multistep 68 min gradient at 200 μL/min flow rate, from fixed 5% B (80% acetonitrile) for 1 min; 5–40% B for 42 min; 40-60% for 8 min; 60–95% for 2 min; fixed 95% for 4 min; then a ramp back 95–5% B for 2 min, holding at 5% for another 10 min. Eluate fractions were collected every minute from 1–61 minutes for a total 60 fractions, which were concatenated into 30 final fractions, dried down, and resuspended in 0.1% formic acid for LC-MS/MS analysis. For the Clicked (SEC) sample, peptides were resuspended in SEC Mobile Phase (0.1% formic acid, 30% acetonitrile) and loaded onto a Superdex peptide PC 3.2/30 column (GE Healthcare). Separation was performed in 60 minutes using an isocratic flow of

Mobile Phase at 0.08 mL/min. After 10 minutes, eluate fractions were collected every 1.875 minutes for a total of 24 fractions. Out of the first 11 fractions, the first 7 were concatenated into 1, and fractions 8, 9, 10, and 11 were kept individually, while fractions 12 through 24 were discarded. Each of the 5 final fractions was submitted to the high pH fractionation and collection method described above. A total of 150 samples were dried and resuspended in 0.1% formic acid for LC-MS/MS analysis.

LC-MS/MS

Data were collected using a Vanquish Neo UHPLC coupled to an Orbitrap Ascend mass spectrometer fronted by an Easy-Spray Source (ThermoFisher Scientific). For the samples in Fig. 4 and the 1xLabeling in Fig. 2A, we also used an Orbitrap Astral mass spectrometer fronted by an Easy-Spray Source (ThermoFisher Scientific). For each sample, approximately 1 μg of peptide mass was injected onto a 300μm x 5 mm PepMap Neo Trap Cartridge peptide trap column (C18, 5μm particle size, 100 Å pore size, ThermoFisher Scientific), which was then submitted to reverse phase chromatography using an EASY-Spray HPLC analytical column (75μm x 50 cm, C_{18}, 2μm particle size, 100 Å pore size, ThermoFisher Scientific) at a flow rate of 250 nL/min at 40 °C. Mobile Phase A consisted of 0.1% (v/v) formic acid in water, while Mobile Phase B consisted of 0.1% (v/v) formic acid in 80:20 acetonitrile: water (v/v).

For monovalent labeled samples, separation was carried out using a multistep 120-minute gradient from 4-30% B for 85 minutes; 30-45% B for 20 minutes; then a 15-minute wash at 99% B. Mass spec data were acquired in positive mode using data-dependent acquisition (DDA) with a 2 second cycle time. Full MS scans were performed in the Orbitrap set at 120,000 resolution (at *m/z* 200) for the 375-1875 m/z range, with maximum injection time set as Auto and normalized AGC target as Standard. Precursors with charge states 2-6+ were selectively isolated (quadrupole isolation window of 1.6 Th) for fragmentation using stepped HCD at Normalized Collision Energies (NCE) of 27, 30, and 33. Global source parameters included spray voltage at 1800V, ion transfer tube set to 275 °C and RF Lens at 60%, the Dynamic exclusion window was set to 10 s. MS^2 scans were performed using the Orbitrap set at 30,000 resolution (*m/z* 200) with maximum injection time set to Auto and AGC target to 1e5. When the Astral was used, parameters were mostly the same, with the MS^2 scan range set at m/z 150-2000, Normalized Collision Energy of 30%, maximum injection time of 10 ms, and AGC target of 300%.

For crosslinked samples (Clicked) coming from fractionation, separation was carried out using a multistep 90 min gradient from 4-20% B for 55 min; 20-45% B for 15 min; then a 20 min wash at 99% B. Gradient was extended to 180 min for the Clicked (SEC) samples. Mass spec data was acquired using DDA in a 2.5 second cycle time using the same source parameters, with a few modifications made to the precursor selection. Full MS scans were performed in the orbitrap set at 120,000 resolution (at m/z 200) for the 375-1875 m/z range, with maximum injection time set to Auto and AGC target at 1e6. Precursors with charge states 4-8+ were selectively isolated (quadrupole isolation window of 1.6 Th) for fragmentation using stepped HCD at Normalized Collision Energies (NCE) of 27, 30, and 33. The dynamic exclusion window was set to 10 s. MS^2 scans were performed using the orbitrap set at 30,000 resolution (m/z 200) with maximum injection time set to Auto and AGC target to 1e5.

Cell staining and imaging for structural analysis

A549 cells grown on glass coverslips were washed with 1X PBS, then fixed and permeabilized as described above. Cells were treated with Reagent **1** and Reagent **2** (1 mM each, added simultaneously) as described in the in situ monovalent labeling protocol, extensively washed with 1X PBS, then submitted to the click-chemistry reaction as described above, except for the labeled (but not clicked) controls. The clicked catalysts were extensively washed out with 5 mM EDTA in 1X PBS.

For phalloidin staining, samples were permeabilized with 0.5% Triton-X-100 for 10 min at 25 °C, then washed with 1X PBS. Cells were stained with 1 mL of CF647-phalloidin (Biotium) at 1:40 v/v in PBS buffer for 60 min in the dark under gentle mixing. Excess phalloidin was removed, and cells were washed. Coverslips were then mounted onto microscope slides with EverBrite + DAPI mounting medium (Biotium) and sealed with clear nail polish and stored at 4 °C in the dark overnight. Cells were imaged using an AxioObserver.Z1 inverted microscope using the 40X oil immersion objective. Images were acquired in the 647 nm and DAPI channels with a 500 ms exposure time using the ZEN microscopy software. Images were pseudo-coloured, and brightness adjusted for merged composites using ImageJ software. The distribution of phalloidin fluorescent intensity was measured across 3 micrographs per condition using the ZEN blue software with a maximum bin count set to 4096 and bin size of 1 for the intensity histogram. The assessment of ultrastructure preservation or distortion came from monitoring select features from approximately 100 cells across 6–7 micrographs: major straited actin filaments, diffusive actin structures, presence of filopodia, and the overall rounding of cell shapes.

For the tubulin immunofluorescent staining, samples were also submitted to a second permeabilization step with 0.5% Triton-X-100 in 1X PBS for 10 min at 25 °C, then washed. Samples were blocked with a 1% BSA (m/v) in 1X PBS solution for 30 min at room temperature. The blocking solution was removed, and cells were stained with a 1:1000 dilution of anti-α-tubulin-FITC mouse monoclonal antibody (Sigma-Aldrich) in 1% BSA + PBS solution for 90 min at room temperature, then washed with 0.05% Tween-20 in 1X PBS. Coverslips were then mounted onto microscope slides with EverBrite + DAPI mounting medium (Biotium) and sealed with clear nail polish and stored at 4 °C in the dark overnight. Cells were imaged using the same microscope as above, using the 40X and 100X oil immersion objectives with 110 ms and 200 ms exposure times, respectively, in the FITC channel and 10 ms exposure time in the DAPI channel using the ZEN microscopy software. Image processing was done the same way as the Phalloidin staining.

Metabolomics analysis

All analyses were performed at The Metabolomics Innovation Centre (Edmonton, Alberta, Canada) using standardized protocols. Briefly, metabolites were extracted (in quadruplicate) from fixed and permeabilized A549 cells, and from live A549 cells as a control, using methanol/water (4:1 v/v). Samples were normalized to 8 mM, then labeled with light $^{12}C_2$ dansylation reagent, and each sample was combined with, and referenced against, to a pooled sample that was labeled with heavy $^{13}C_2$ dansylation reagent for normalization purposes. Samples were run on a Bruker Impact II QTOF (positive ion mode, m/z range 220-1000, 1 Hz acquisition rate) outfitted with a Thermo Scientific Vanquish LC using mobile phase A (0.1% formic acid in water) and mobile phase B (0.1% formic acid in acetonitrile). Separation was achieved using a gradient of B, starting at 25% (t = 0 min) and ending at 99% (t = 15 min), at a flow rate of 400 μl/min. Metabolites were identified by library match to the CIL library, the LI library, and the MyCompoundID library, using accurate mass and retention time, generating 1814 identifications (or putative matches) from 2028 unique peak pairs.

Monovalent data analysis

Monovalent labeling efficiency was assessed using MSFragger inside FragPipe (v22.0)[37]. For every sample, we performed an OpenMod search to investigate which labeling tags were being installed into proteins by the different reagents used, and if there were any unexpected side products we did not anticipate. The OpenMod search was conducted against the full Escherichia coli proteome (UniProt

database, retrieved September 2021) or the full Homo sapiens proteome (UniProt database, retrieved February 2023) with mostly default parameters. Notable changes include the MS^1 range from -150 to 650 Da, MS^2 error tolerance 15ppm, inclusion of cysteine alkylation as a variable modification instead of a fixed. After confirming the mass shifts, the LFQ-MBR workflow was used to investigate the quantitative proportion of labeled versus unlabeled peptides and thus estimating reaction performance according to the following equation:

$$\%\text{Labeling} = \frac{\sum \text{XIC(Labeled peptides)}}{\sum \text{XIC(All peptides)}} \times 100 \quad (1)$$

The LFQ-MBR search routine was also performed against the full proteome databases with the following parameters: cysteine carbamidomethylation (Δm = +57.021465 Da) as fixed modification; methionine oxidation (Δm = +15.9949 Da) and N-termini acetylation (Δm = +42.0106 Da) as variable modifications; 10 ppm for precursor mass tolerance; 15 ppm for fragment mass tolerance; trypsin as enzyme for protein digestion with 3 allowed missed cleavages. The mass shifts corresponding to the reagent modification were adjusted for every molecule as follows: Reagent **1** (Δm = 110.0366 Da), Reagent **2** (Δm = 139.0745 Da), DBCO-Capped-Azide (Δm = 444.1798 Da), Reagent 1 clicked with Azide-PEG2-Alcohol (Δm = 285.1324 Da). IonQuant was used for label-free quantitation, and each mass spec run was processed individually.

Crosslinking data analysis

After clicking, we monitored the residual non-clicked monolinks using the same pipeline described above through FragPipe. Crosslinking data analysis was performed using pLink 2.3.11[38]. Parameters used were as follows: peptide length 6–60; trypsin as the digestion enzyme with 3 allowed missed cleavages; carbamidomethylation of cysteines (Δm = +57.021 Da) as a fixed modification; oxidation of methionine (Δm = +15.995 Da) as a variable modification; 5 ppm for precursor and 10 ppm for fragment mass tolerance. Data were searched against the full UniProt Human proteome databases at 5% false discovery rate (FDR) at the spectrum level. Crosslink (Δm = +249.111 Da) and monolink modifications were added for the clicked products, with specificity towards Lysine residues and protein N-termini (only one monolink is allowed on pLink, we selected the more abundant Reagent **1** at Δm = +110.037 Da).

For comparison of trends, data was also searched using pLink v3.0.17, CRIMP v2.0 inside Mass Spec Studio and MS Annika v3.0 inside Proteome Discoverer 3.1, the only tools capable of searching against the entire human proteome. For pLink3, parameters used were the same as from pLink2 described above. For CRIMP, parameters used were mostly default with the exception of: carbamidomethylation of cysteines (Δm = +57.021 Da) as a fixed modification; oxidation of methionine (Δm = +15.995 Da) as a variable modification; 5 ppm for precursor and 10 ppm for fragment mass tolerance, minimum fragment threshold = 3, maximum and minimum isolation window = 0.8, % E-Threshold = 50%. For MS Annika, parameters were mostly the same as the provided workflow template for DSS/BS3 MS^2 searches of large datasets with few modifications, namely: 5ppm for MS1 tolerance, 10ppm for MS^2 tolerance; static modification of cysteine carbamidomethylation (Δm = +57.021 Da); dynamic modifications of methionine oxidation (Δm = +15.995 Da) as well as respective monolinks (hydrolyzed and Tris-quenched for DSS and PhoX, Reagent 1 and Reagent 2 precursors for Click-Linking); peptide length 5-30; TopN Filter 5; Separate Intra/Inter-link FDR set to False.

The output from all conditions and all search tools was searched against the STRING human protein interaction database (v12.0, retrieved March 2024) using an in-house developed Python script. The large Click-Linking (SEC) dataset was also mapped into protein structures using CLAUDIO[32], which is capable of mapping crosslinks both into known structures from the PDB[39] and to AlphaFold-generated models[40] when a high-resolution experimental structure is not available.

Cellular compartment co-localization analysis

Gene-ontology terms for proteins involved in PPIs were retrieved from the Uniprot database, and the number of PPIs with one or more shared cellular compartment(s) was quantified using an in-house script, as a function of STRING score. To estimate how frequently shared compartments could be observed by chance, we pulled 1,736 proteins from the human proteome at random, then randomly assigned pairs to a PPI for compartment evaluation. This process was performed in triplicate, and the results were averaged.

Determination of Reagent-accessible surface area

Reagent residue accessibility was determined using *freesasa*[41], using publicly available structure predictions, which were accessed via RCSB[42,43]. Predictions were solely from AlphaFold2 (version 4)[40]. Residue accessibility was calculated for all proteins whose structures were available. Peptides were aligned to the structure where required. The reagent accessibility was calculated using the Lee Richards algorithm for solvent accessibility, using a probe radius which was derived from the literature surface area of Succinimidyl Acetate (63.7Å^2; probe radius = 4.3 Å). The result of this calculation is 0 when the measured entity (e.g., residue or atom) is completely occluded from the reagent in the static structure.

Reporting summary

Further information on research design is available in the Nature Portfolio Reporting Summary linked to this article.

Data availability

The crosslinking and labeling data generated in this study have been deposited in the PRIDE partner repository[44] with the dataset identifier PXD059118 [http://proteomecentral.proteomexchange.org/cgi/GetDataset?ID=PXD059118. Source data are provided with this paper.

References

1. Snider, J. et al. Fundamentals of protein interaction network mapping. *Mol. Syst. Biol*. **11**, 848 (2015).
2. Liu, X., Abad, L., Chatterjee, L., Cristea, I. M. & Varjosalo, M. Mapping protein–protein interactions by mass spectrometry. *Mass Spectrom. Rev*. https://doi.org/10.1002/MAS.21887 (2024).
3. Cronan, J. E. Biotin protein ligase as you like it: Either extraordinarily specific or promiscuous protein biotinylation. *Proteins* **92**, 435–448 (2024).
4. Baryshev, A. et al. Massively parallel measurement of protein–protein interactions by sequencing using MP3-seq. *Nat. Chem. Biol*. **20**, 1514–1523 (2024).
5. Johnson, K. L. et al. Revealing protein-protein interactions at the transcriptome scale by sequencing. *Mol. Cell* **81**, 4091–4103.e9 (2021).
6. Belsom, A. & Rappsilber, J. Anatomy of a crosslinker. *Curr. Opin. Chem. Biol*. **60**, 39–46 (2021).
7. Botticelli, L. et al. Chemical cross-linking and mass spectrometry enabled systems-level structural biology. *Curr. Opin. Struct. Biol*. **87**, 102872 (2024).
8. Iacobucci, C., Götze, M. & Sinz, A. Cross-linking/mass spectrometry to get a closer view on protein interaction networks. *Curr. Opin. Biotechnol*. **63**, 48–53 (2020).
9. Stahl, K., Graziadei, A., Dau, T., Brock, O. & Rappsilber, J. Protein structure prediction with in-cell photo-crosslinking mass spectrometry and deep learning. *Nat. Biotechnol*. **41**, 1810–1819 (2023).
10. Stahl, K. et al. Modelling protein complexes with crosslinking mass spectrometry and deep learning. *Nat. Commun*. **15**, 7866 (2024).

11. Zhu, Y. et al. Cross-link assisted spatial proteomics to map sub-organelle proteomes and membrane protein topologies. *Nat. Commun.* **15**, 3290 (2024).
12. Wheat, A. et al. Protein interaction landscapes revealed by advanced in vivo cross-linking-mass spectrometry. *Proc. Natl. Acad. Sci. USA.* **118**, e2023360118 (2021).
13. Bakhtina, A. A., Wippel, H. H., Chavez, J. D. & Bruce, J. E. Combining Quantitative Proteomics and Interactomics for a Deeper Insight into Molecular Differences between Human Cell Lines. *J. Proteome Res.* https://doi.org/10.1021/ACS.JPROTEOME.4C00503 (2024).
14. Lenz, S. et al. Reliable identification of protein-protein interactions by crosslinking mass spectrometry. *Nat. Commun.* **12**, 3564 (2021).
15. Lee, K. & O'Reilly, F. J. Cross-linking mass spectrometry for mapping protein complex topologies in situ. *Essays Biochem.* **67**, 215–228 (2023).
16. Michael, A. R. M., Amaral, B. C., Ball, K. L., Eiriksson, K. H. & Schriemer, D. C. Cell fixation improves performance of in situ crosslinking mass spectrometry while preserving cellular ultra-structure. *Nat. Commun.* **15**, 8537 (2024).
17. Stumpf, M. P. H. et al. Estimating the size of the human interactome. *Proc. Natl Acad. Sci. USA.* **105**, 6959–6964 (2008).
18. Claude Bernard Lyon, U. et al. Kinetic principles of chemical cross-link formation for protein–protein interactions. *Proc. Natl Acad. Sci.* **121**, e2402040121 (2024).
19. Luu, T., Gristwood, K., Knight, J. C. & Jörg, M. Click Chemistry: Reaction Rates and Their Suitability for Biomedical Applications. *Bioconjug. Chem.* **35**, 715–731 (2024).
20. Rodionov, V. O., Presolski, S. I., Díaz, D. D., Fokin, V. V. & Finn, M. G. Ligand-accelerated Cu-catalyzed azide-alkyne cycloaddition: A mechanistic report. *J. Am. Chem. Soc.* **129**, 12705–12712 (2007).
21. Agard, N. J., Prescher, J. A. & Bertozzi, C. R. A strain-promoted [3 + 2] azide-alkyne cycloaddition for covalent modification of biomolecules in living systems. *J. Am. Chem. Soc.* **126**, 15046–15047 (2004).
22. Soriano Del Amo, D. et al. Biocompatible copper(I) catalysts for in vivo imaging of glycans. *J. Am. Chem. Soc.* **132**, 16893–16899 (2010).
23. Wiest, A. & Kielkowski, P. Cu-catalyzed azide-alkyne-thiol reaction forms ubiquitous background in chemical proteomic studies. *J. Am. Chem. Soc.* **146**, 2151–2159 (2024).
24. Kamps, J. J. A. G., Hopkinson, R. J., Schofield, C. J. & Claridge, T. D. W. How formaldehyde reacts with amino acids. *Commun. Chem.* **2**, 1–14 (2019).
25. DesMarais, V., Eddy, R. J., Sharma, V. P., Stone, O. & Condeelis, J. S. Optimizing Leading Edge F-Actin labeling using multiple actin probes, fixation methods and imaging modalities. *Biotechniques* **66**, 113–119 (2019).
26. Faulstich, H., Zobeley, S., Heintz, D. & Drewes, G. Probing the phalloidin binding site of actin. *FEBS Lett.* **318**, 218–222 (1993).
27. Kim, E. & Reisler, E. Intermolecular coupling between loop 38-52 and the C-terminus in actin filaments. *Biophys. J.* **71**, 1914–1919 (1996).
28. Steigenberger, B., Pieters, R. J., Heck, A. J. R. & Scheltema, R. A. PhoX: An IMAC-enrichable cross-linking reagent. *ACS Cent. Sci.* **5**, 1514–1522 (2019).
29. Neumann, S., Biewend, M., Rana, S. & Binder, W. H. The CuAAC: Principles, Homogeneous and Heterogeneous Catalysts, and Novel Developments and Applications. *Macromol. Rapid Commun.* **41**, 1900359 (2020).
30. Birklbauer, M. J. et al. Proteome-wide non-cleavable crosslink identification with MS Annika 3.0 reveals the structure of the C. elegans Box C/D complex. *Commun. Chem.* **7**, 300 (2024).
31. Crowder, D. A. et al. High-Sensitivity Proteome-Scale Searches for Crosslinked Peptides Using CRIMP 2.0. *Anal. Chem.* **95**, 6425–6432 (2023).
32. Rohl, A., Netz, E., Kohlbacher, O. & Elhabashy, H. CLAUDIO: automated structural analysis of cross-linking data. *Bioinformatics* **40**, btae146 (2024).
33. Schwerk, C. et al. ASAP, a Novel Protein Complex Involved in RNA Processing and Apoptosis. *Mol. Cell. Biol.* **23**, 2981 (2003).
34. Tange, T., Shibuya, T., Jurica, M. S. & Moore, M. J. Biochemical analysis of the EJC reveals two new factors and a stable tetrameric protein core. *RNA* **11**, 1869–1883 (2005).
35. Hir, H., Le, Saulière, J. & Wang, Z. The exon junction complex as a node of post-transcriptional networks. *Nat. Rev. Mol. Cell Biol.* **17**, 41–54 (2016).
36. Murachelli, A. G., Ebert, J., Basquin, C., Le Hir, H. & Conti, E. The structure of the ASAP core complex reveals the existence of a Pinin-containing PSAP complex. *Nat. Struct. Mol. Biol.* **19**, 378–386 (2012).
37. Kong, A. T., Leprevost, F. V., Avtonomov, D. M., Mellacheruvu, D. & Nesvizhskii, A. I. MSFragger: ultrafast and comprehensive peptide identification in mass spectrometry–based proteomics. *Nat. Methods* **14**, 513–520 (2017).
38. Chen, Z. L. et al. A high-speed search engine pLink 2 with systematic evaluation for proteome-scale identification of cross-linked peptides. *Nat. Commun.* **10**, 1–12 (2019).
39. Berman, H. M. et al. The Protein Data Bank. *Nucleic Acids Res.* **28**, 235–242 (2000).
40. Jumper, J. et al. Highly accurate protein structure prediction with AlphaFold. *Nature* **596**, 583–589 (2021).
41. Mitternacht, S. FreeSASA: An open source C library for solvent accessible surface area calculations. *F1000Research* **5**, 189 (2016).
42. Bittrich, S. et al. RCSB Protein Data Bank: Efficient searching and simultaneous access to one million computed structure models alongside the PDB structures enabled by architectural advances. *J. Mol. Biol.* **435**, 167994 (2023).
43. Rose, Y. et al. RCSB protein data bank: architectural advances towards integrated searching and efficient access to macromolecular structure data from the PDB archive. *J. Mol. Biol.* **433**, 166704 (2021).
44. Deutsch, E. W. et al. The ProteomeXchange consortium at 10 years: 2023 update. *Nucleic Acids Res.* **51**, D1539–D1548 (2023).
45. Huang, Q., Szklarczyk, D., Wang, M., Simonovic, M. & Mering, C. von. PaxDb 5.0: curated protein quantification data suggests adaptive proteome changes in yeasts. *Mol. Cell. Proteom.* **22**, 100640 (2023).

Acknowledgements

This work was funded by the Natural Sciences and Engineering Research Council of Canada Discovery Grants RGPIN 2017-04879 to D.C.S. All figures created and/or assembled with BioRender.com, released under a Creative Commons Attribution-NonCommercial-NoDerivs 4.0 International license.

Author contributions

D.C.S., B.C.A., and A.R.M.M. conceptualized the project and designed experiments. A.R.M.M. collected all imaging data. B.C.A., N.I.B,. and A.R.M.M. collected all mass spectra data, with assistance from K.H.E.. B.C.A.analyzed all data. D.A.C. generated the scripts and performed the surface-accessibility analysis. D.C.S. and B.C.A. generated the first draft of the manuscript, and all authors helped finalize the paper.

Competing interests

The authors declare no competing interests.

Additional information

Supplementary information The online version contains supplementary material available at https://doi.org/10.1038/s41467-025-64888-9.

Correspondence and requests for materials should be addressed to David C. Schriemer.

Peer review information *Nature Communications* thanks the anonymous reviewer(s) for their contribution to the peer review of this work. A peer review file is available.